ChemComm

Accepted Manuscript

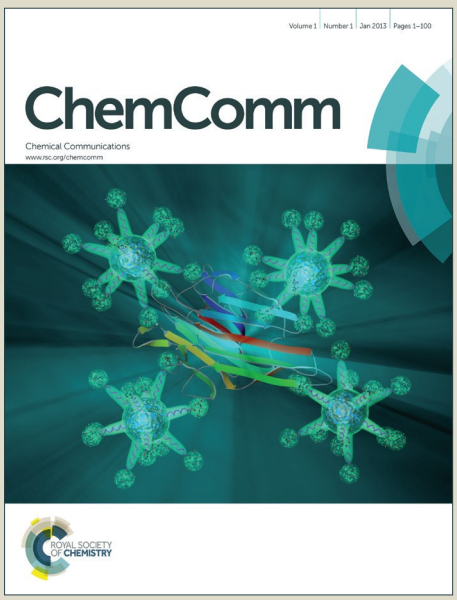

ROYAL SOCIETY OF CHEMISTRY

www.rsc.org/chemcomm

Chemical Communcations

COMMUNICATION

Dendrimer Porphyrin-coated Gold Nanoshell for Synergistic Combination of Photodynamic and Photothermal Therapy

Received 00th January 20xx,
Accepted 00th January 20xx

DOI: 10.1039/x0xx00000x

www.rsc.org/

Ui Seok Chung[a], Joo-Ho Kim[b], Byeonggwan Kim[a], Eunkyoung Kim[a], Woo-Dong Jang[b,*], and Won-Gun Koh[a,*]

Dendrimer porphyrin (DP)-coated gold nanoshell (AuNS-DP) was prepared for synergistic combination of photodyanmic and photothermal therapy. The resultant AuNS-DP succesfully exhibited generation of reactive oxygen species (ROS) as well as photothermal effect for simultanous applicaton of photodynamic therapy (PDT) and photothermal therapy (PTT).

Phototherapy has attracted considerable attention as a non-invasive therapeutic technique for cancer treatment due to its unique advantages such as remote controllability, improved selectivity, and low systemic toxicity.[1] Phototherapies induced by visible or near infrared (NIR) light usually involve phototherapeutic agents that have little toxicity in the dark, but are able to selectively kill cancer cells when exposed to light irradiation without causing much damage to normal tissues. Photodynamic therapy (PDT) and photothermal therapy (PTT), two different types of phototherapy that are commonly used for therapeutic purposes, require the absorption of incoming light by a photosensitizer (PS) or photothermal agent (PTA) to generate reactive oxygen species (ROS) or heat to kill cancer cells, respectively.[2]

The photodynamic efficacy of PS formulations would be the most important point for the effective PDT. Among various PSs, porphyrin is the most extensively used PS.[3] However, PDT often gives unsatisfactory results due to the limitations of PSs. Therefore, combination of PDT with PTT attracts interests because both therapies utilize radiation of nontoxic low energy photons.[4] Because PDT and PTT give absolutely different effect on the tumour cells, the combination of those two treatments possibly give synergistic effects. However, the combination of PDT and PTT has an inherent problem. PDT is based on the excitation energy transfer from PSs to molecular oxygen, but PTT is based on the thermal relaxation of excitation energy of PTA. Since these two different mechanisms are controversial to each other, direct conjugation of PS and PTA results in efficient excitation energy transfer from PS to PTA, which significantly decreases the efficacy of ROS generation by quenching between PS and PTA.[2,4,5] Many nanocomplexes have been developed to minimize the excitation energy transfer from PSs to PTA for effective combined phototherapy of PDT and PTT by leaving the space between PS and PTA or releasing quenched PS from nano-complexes.[4c, 6]

We have previously reported negatively charged dendrimer porphyrin (DP; Figure S1) that exhibit excellent PDT efficacy.[7] Unlike other forms of PSs, the presence of large dendritic wedges in DP can effectively segregate the photofunctional focal porphyrin and thereby prevent the collisional quenching of the porphyrins, even at very high concentrations.[8] We also hypothesize that the dendritic wedge can play a role as spacer between porphyrin and PTA to minimize the energy transfer and subsequent quenching of PS.

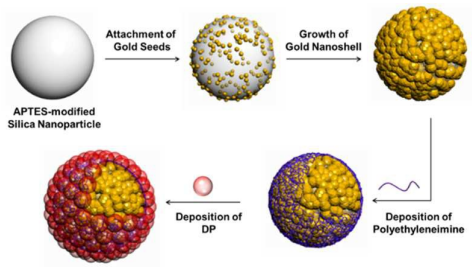

Figure 1. Schematic illustration of the preparation of the multilayered nanoparticles consisting of gold nanoshell and dendrimer porphyrin on the silica nanoparticles.

For the synergistic combination of PDT and PTT, we fabricated gold nanoshell (AuNS) onto the silica nanoparticles (SNP), and DP was immobilized by layer-by-layer (LbL) deposition with polyethyeneimine (PEI) as shown in Figure 1. For the preparation of DP-coated AuNS (AuNS-DP), AuNS were fabricated by deposition of tiny gold seeds and subsequent seed growth on the SNPs. Prior to the deposition of the gold

[a] *Department of Chemical and Biomolecular Engineering, Yonsei University, 50 Yonsei-ro, Seodaemoon-gu, Seoul 120-749, Republic of Korea*
[b] *Department of Chemistry, Yonsei University, 50 Yonsei-ro, Seodaemoon-gu, Seoul 120-749, Republic of Korea.*
** Author to whom correspondence should be addressed.*
Prof. Woo-Dong Jang E-mail: wdjang@yonsei.ac.kr, Prof. Won-Gun Koh, E-mail: wongun@yonsei.ac.kr
Electronic Supplementary Information (ESI) available: [Experimental details]. See DOI: 10.1039/x0xx00000x

seeds, the SNPs were functionalized with (3-aminopropyl) triethoxysilane (APTES) to facilitate the attachment of the gold seeds. After APTES treatment, the ς-potential of the SNPs was changed from - 34.4 to +17.3 mV at pH 7.4. At this pH value, APTES bears a net positive charge because its isoelectric point (pI) is approximately 8.7. The terminal amine groups of APTES act as the attachment points for the tetrakis(hydroxymethyl)-phosphonium chloride (THPC)-stabilized gold seed with a mean diameter of 1-2 nm. The gold seed can attach to the APTES-modified surfaces stably not only by coordinating with the lone pairs of the terminal amine groups but also by electrostatic attraction between the negatively charged THPC-stabilized gold seed and positively charged APTES-modified SNPs.[9] The gold seeds were evenly distributed on the surface of the APTES-modified SNPs, and the resultant gold seeds-decorated SNPs exhibited a small absorbance peak at 540 nm, which arises from the surface plasmon absorbance of the AuNPs (Figure S2).

Further gold coverage of the SNPs was achieved by the reduction of gold hydroxide by hydroxylamine hydrochloride on the SNP surface. Here, the initially attached gold seeds served as nucleation sites for the coalescence of the gold seeds, generating gold nanoshell on the SNP (AuNS). Formation of AuNS was first confirmed by a colour change of the nanoparticle-containing solution. The colour of the initial gold seed-coated SNP solution was brown, and it changed to purple and then to blue-green as the coverage of the AuNS increased (Figure 2a). The TEM images shown in Figure 2b also confirm the formation of AuNS and indicate that the surface coverage of the gold is dependent on the amount of the gold hydroxide solution. When the amount of gold hydroxide was increased, the gold seed on the SNPs became larger, which subsequently increased the gold coverage. When the gold hydroxide addition was reached to 0.250 mM, fairly thick AuNS was obtained and the shape was persisted even after dissolution of SNP. To remove the SNP core, AuNS was immersed in 5 M hydrofluoric acid (HF) buffered with 13.3 M ammonium fluoride at a volumetric ratio of 1:1.5. SEM and TEM images (Figure S3) showed the formation of hollow AuNS after dissolution of SNP cores.

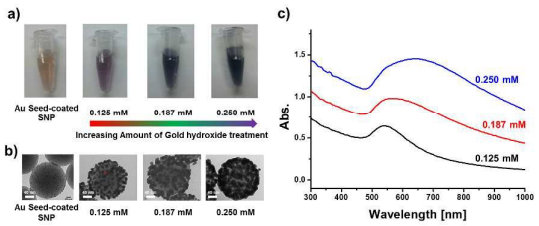

Figure 2. Formation of gold nanoshell on the silica nanoparticles (AuNS) with different amounts of gold hydroxide treatment. a) Color change of the AuNS-containing solution, b) TEM images of the AuNS, and c) electronic absorptions of AuNS.

The increase in gold coverage resulted in wider (600 ~ 800 nm) and red-shifted absorbance peaks of solution, as shown in Figure 2c. Therefore, the final product of AuNS (made from 20 mL of gold hydroxide) could absorb visible light as well as near infrared (NIR) light.

DP was incorporated onto the AuNS via an LbL deposition method. The final form of the AuNS exhibited a negative ζ-potential value (-10.8 mV) at pH 7.4 due to the phosphate groups of the THPC. Because of the negative surface potential, self-assembled layers can be prepared on the surface of AuNS through the alternate deposition of positive and negative electrolytes by means of electrostatic attraction. DP has a negative ζ-potential (-31 mV) due to the peripheral carboxylate group, and therefore can play a role as a negative electrolyte. Positively charged PEI and negatively charged DP were alternately deposited onto AuNS to obtain AuNS-DP. As shown in Figure 3a, deposition of PEI and DP resulted in positive and negative ζ-potential values, respectively, which indicates that the surface layer was charge-overcompensated in each deposition step and enabled the PEI/DP bilayer to form. Formation of the PEI/DP bilayer was also confirmed with an absorbance measurement, which was accomplished because the porphyrin unit in the DP core has an absorbance peak of approximately 430 nm (Soret band of porphyrin) (Figure 3b). The amount of DP within the multilayer could be easily controlled by altering the repeating number of the LbL deposition. As shown in Figure 3b, the absorbance of the AuNS-DP increased with an increasing number of bilayers due to the presence of more DP in the multilayers. Although the amount of DP, which is the strength of the PDT effect, could be easily controlled by adjusting the number of deposited layer.[7a] We only used one bilayer of PEI and DP for rest of this study to highlight the effect of combination therapy. For the control experiment of PDT, DP-coated SNPs (SNP-DP) were prepared by alternative deposition of PEI and DP onto negatively charged bare SNPs.

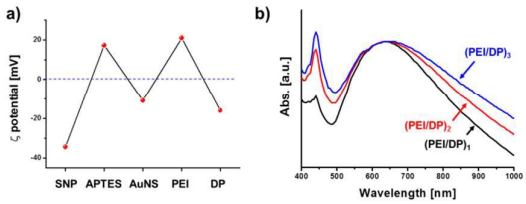

Figure 3. Preparation of AuNS-DP. The presence of DP on the AuNS after LbL deposition was confirmed by measuring the ς-potential and the absorbance. a) The change of the ς-potential of the silica nanoparticles after the deposition of different materials, and b) electronic absorption of the AuNS-DP with different LbL layers of PEI and DP.

Four different nanoparticles (SNP, AuNS, SNP-DP, and AuNS-DP) was further investigated with dynamic light scattering (DLS) measurement and thermogravimetric analysis (TGA) (Figure S4). DLS results reveals that average sizes of SNP, SNP-DP, AuNS, and AuNS-DP were 167.8, 171.7, 181.4, and to 186.2 nm, respectively, which confirm the increase of nanoparticle size due to the deposition of gold layer and DP (Figure S4a). TGA analysis exhibited very small decrease of weight for SNPs and AuNS due to lack of organic compounds in both nanoparticles. On the other hands, there was approximately 14% weight decrease for SNP-DP and AuNS-DP, which was attributed mainly by removal of DP. Therefore, these results

from DLS and TGA analysis also demonstrate the successful deposition of gold layer and DP onto SNP.

PTT effect of the formulations was evaluated by measuring the temperature change under 808 nm NIR laser irradiation. After a 5 min of NIR exposure, a solution containing AuNS or AuNS-DP was rapidly heated to over 50 °C due to a high NIR absorptivity of gold layer (Figure S5a), while the solution containing SNP or SNP-DP showed much less photothermal heating. The temperature change of the nanoparticle-containing solution was also monitored under visible light. Although continuous increases in temperature have been observed, the degree of temperature elevations upon visible light exposure was very smaller than those upon NIR exposure. Similar to the temperature increase seen with NIR exposure, the temperature of the solution containing AuNS or AuNS-DP increased more rapidly than the solution of SNP or SNP-DP upon exposure to visible light (Figure S5b).

To examine the ROS generation, HeLa cells were incubated with four different nanoparticles (SNP, AuNS, SNP-DP, AuNS-DP) and subsequently irradiated with visible light for 15 minutes. Firstly, intracellular localization of AuNS-DP were investigated by TEM. As shown in Figure 4a, AuNS-DP clearly showed cell internalization by endocytosis, where the red arrows indicate endosomal compartments. The intracellular ROS generation was evaluated with H2DCFDA, a standard probe to detect ROS.[10] A strong green fluorescence signal indicating ROS generation was detected in HeLa cells treated with AuNS-DP, while there was very weak fluorescence signal in the cells incubated with SNPs and treated with light irradiation (Figure 4b). Quantification of the fluorescence intensity revealed that much higher intracellular ROS levels were observed in irradiated cells that were incubated with DP-containing nanoparticles such as SNP-DP and AuNS-DP than cells incubated with DP-free nanoparticles such as SNP and AuNS (Figure 4c). These results demonstrate that the DPs in the nanoparticles could successfully generate ROS upon light irradiation.

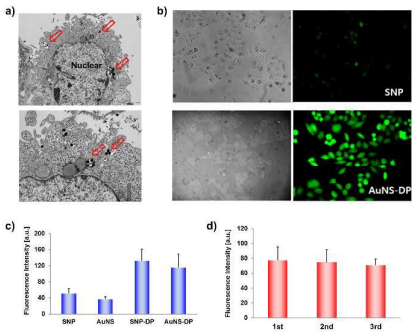

Figure 4. *In vitro* observations of AuNS-DP treated cells. a) TEM images of HeLa cells treated with AuNS-DP, b) fluorescence and optical images indicating ROS generation in HeLa cells treated with AuNS-DP and light irradiation, c) quantification of generated ROS using fluorescence intensity, and d) relative ROS generation from AuNS-DP after repeated light exposure.

As aforementioned, the presence of gold nanostructures near the PS such as porphyrin within nanocomplex usually results in the significant decrease of ROS generation due to the energy transfer between gold and PS. In order to maximize the ROS generation from nanocomplex consisting of gold and PS, most of combination phototherapy used PTT followed by PDT, where quenched PS was released from nanocomplex via external stimulus, and subsequently dequenched and capable of generating ROS. However, in our system, ROS levels from AuNS-DP were similar with that from SNP-DP. There are two possible reasons for this result. One is that DP can be released from AuNS-DP and generate ROS, avoiding quenching by AuNS. The other is that dendritic wedge in DP leave the space between porphyrin (PS) and AuNS (PTA), minimizing the quenching of PS. We investigated whether AuNS-DP, that was exposed to light and generated ROS, could be regenerate ROS upon repeated light exposure. As shown in Figure 4d, AuNS-DP maintained its capability to generate almost same level of ROS during repeated light irradiation and washing steps. This result indicates that negatively-charged dendritic wedge in DP not only allowed porphyrin to remain to nanoparticles without releasing but also provide space between porphyrin and gold so that it enable porphyrin to repeatedly generate ROS upon light irradiation with quenching. Because fluorescence was observed only inside the cells, it can be inferred that the AuNS-DP were taken up and internalized by the cells. When NIR was used instead of visible light, no significant ROS level was detected even from DP-containing nanoparticles (data not shown), indicating that generation of ROS mainly results from absorption of visible light by DP. According to these results, the AuNS-DP is able to not only generate ROS but also induce photothermal heating upon exposure to visible light. Therefore, it was hypothesized that a combination of both the photothermal and photodynamic effects would be achievable with AuNS-DP using only visible light, and a further photothermal effect would be obtained by subsequent NIR exposure.

Cytotoxicity of the SNP, SNP-DP, AuNS, and AuNS-DP under a dark condition was evaluated. As shown in Figure 5a, all of the nanoparticles showed good cytocompatibility (> 80%) over the entire concentration range. After confirming that sequential irradiation of visible light for 15 minutes and NIR for 5 minutes in cells cultured without nanoparticles or with bare SNP did not cause any significant damage on cell viability, we evaluated the effects of PDT, PTT, and a combined PDT+PTT treatment on tumor cells by incubating HeLa cells with SNP-DP, AuNS, and AuNS-DP followed by photoirradiation. For the evaluation of PDT alone, cells cultured with SNP-DP were exposed to visible light. For the evaluation of PTT alone, cells cultured with AuNS were exposed to either visible light or NIR. For the evaluation of the combination therapy, cells cultured with AuNS-DP were exposed to only visible light or visible light and NIR. Figure 5b summarizes the cytotoxicity effects induced by PDT, PTT, or PDT+PTT. A higher cytotoxicity was observed for all of the approaches as the concentration of nanoparticles was increased. However, a further increase in the amount of nanoparticles over a certain concentration did not cause additional cytotoxicity for all cases. The cytotoxicity observed was in the following order: (SNP-DP + visible light) < (AuNS +

visible light) < (AuNS + NIR) < (AuNS-DP + visible light) < (AuNS-DP + visible light & NIR). For example, at a 200 μg/mL nanoparticle concentration, PDT alone decreased the cell viability to 80%. Because a 15 minute irradiation of visible light of SNP-DPs did not induce a significant temperature increase, the observed cytotoxicity mainly resulted from ROS generated from the DP. In contrast, PTT alone resulted in a cell viability of 72 and 54% by visible light and NIR treatment, respectively, confirming that a photothermal effect from the AuNS can be achieved by visible light as well as NIR light. When cells incubated with AuNS-DP were exposed to visible light, the cell viability significantly decreased to 45% due to the combined effect of PDT and PTT.

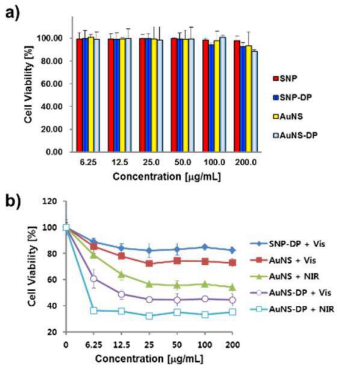

Figure 5. In vitro cytotoxicity assay. a) The dark toxicity of SNPs, SNP-DP, AuNS, and AuNS-DP at various concentrations and b) relative viability of HeLa cells incubated with various concentrations of SNP-DP, AuNS, and AuNS-DP after exposure to visible light (Vis) or/and NIR.

It is notable that even a single irradiation of visible light without NIR synergistically enhanced the cytotoxic effects on the cancer cells via the combination of PDT and PTT compared with the cytotoxic effects of PDT alone from visible light or PTT alone from visible light or NIR light. The highest amount of cell death, where cell viability was 35%, was achieved by the sequential exposure of visible light and NIR light to the cells incubated with AuNS-DPs. It should also be noted that a higher anti-cancer effect was achieved with a much lower dosage for the combination therapy than the single therapy. These results demonstrate that the combination of PDT and PTT treatment caused a significant increase in cell death compared with treatment with PDT alone or PTT alone, which clearly shows a synergistic effect of the two different therapeutic modalities.

In summary, the combination of the PDT effects, resulting from the incorporated DP, and the subsequent PTT effects, resulting from the AuNS, showed a significant increase in the killing efficiency of the AuNS-DP compared to PDT alone or PTT alone. Because of the synergistic effects of the dual phototherapies, a higher anti-cancer effect can be achieved with a much lower dosage, at which a single-modal nanoparticle would have no therapeutic efficacy. Therefore, we believe that this dual-photoactive nanoparticle with a synergistic therapeutic capability has great potential to improve the current cancer phototherapy results.

This work was supported by the Priority Research Centers Programs (2009-0093823), Active Polymer Center for Pattern Integration at Yonsei University (2007-0056091) and Mid-Career Researcher Program (2014R1A2A1A10051083) through National Research Foundation of Korea (NRF).

Notes and references

1 a) L. Cheng, C. Wang, L. Feng, K. Yang and Z. Liu, *Chem. Rev.*, 2014, **114**, 10869-10939; b) G. Saravanakumar, J. Lee, J. Kim and W. J. Kim, *Chem. Commun.*, 2015.

2 a) D. Jaque, L. Martinez Maestro, B. del Rosal, P. Haro-Gonzalez, A. Benayas, J. L. Plaza, E. Martin Rodriguez and J. Garcia Sole, *Nanoscale*, 2014, **6**, 9494-9530; b) P. Agostinis, K. Berg, K. A. Cengel, T. H. Foster, A. W. Girotti, S. O. Gollnick, S. M. Hahn, M. R. Hamblin, A. Juzeniene, D. Kessel, M. Korbelik, J. Moan, P. Mroz, D. Nowis, J. Piette, B. C. Wilson and J. Golab, *CA Cancer J. Clin.*, 2011, **61**, 250-281; c) D. E. J. G. J. Dolmans, D. Fukumura and R. K. Jain, *Nat. Rev. Cancer*, 2003, **3**, 380-387.

3 a) K. Berg, P. K. Selbo, A. Weyergang, A. Dietze, L. Prasmickaite, A. Bonsted, B. O. Engesaeter, E. Angell-Petersen, T. Warloe, N. Frandsen and A. Hogset, *J. Microsc.*, 2005, **218**, 133-147; b) K. Ravindra and G. Zheng, *The porphyrin handbook*, 1999, **6**, 157-161.

4 a) B. Jang, J.-Y. Park, C.-H. Tung, I.-H. Kim and Y. Choi, *ACS Nano*, 2011, **5**, 1086-1094; b) B. Khlebtsov, E. Panfilova, V. Khanadeev, O. Bibikova, G. Terentyuk, A. Ivanov, V. Rumyantseva, I. Shilov, A. Ryabova, V. Loshchenov and N. G. Khlebtsov, *ACS Nano*, 2011, **5**, 7077-7089; c) W. S. Kuo, Y. T. Chang, K. C. Cho, K. C. Chiu, C. H. Lien, C. S. Yeh and S. J. Chen, *Biomaterials*, 2012, **33**, 3270-3278; d) M. Trapani, A. Romeo, T. Parisi, M. T. Sciortino, S. Patanè, V. Villari and A. Mazzaglia, *RSC Advances*, 2013, **3**, 5607; e) P. Vijayaraghavan, C. H. Liu, R. Vankayala, C. S. Chiang and K. C. Hwang, *Adv. Mater.*, 2014, **26**, 6689-6695; f) S. Wang, P. Huang, L. Nie, R. Xing, D. Liu, Z. Wang, J. Lin, S. Chen, G. Niu, G. Lu and X. Chen, *Adv. Mater.*, 2013, **25**, 3055-3061; g) J. Oh, H.-J. Yoon and J.-H. Park, *J. Mater. Chem. B*, 2014, **2**, 2592.

5 J. Y. Kim, W. I. Choi, M. Kim and G. Tae, *J. Control. Release*, 2013, **171**, 113-121.

6 a) J. Wang, G. Z. Zhu, M. X. You, E. Q. Song, M. I. Shukoor, K. J. Zhang, M. B. Altman, Y. Chen, Z. Zhu, C. Z. Huang and W. H. Tan, *ACS Nano*, 2012, **6**, 5070-5077; b) J. F. Lovell, T. W. Liu, J. Chen and G. Zheng, *Chem. Rev.*, 2010, **110**, 2839-2857; c) S. Wang, L. Zhang, C. Dong, L. Su, H. Wang and J. Chang, *Chem. Commun.*, 2015, **51**, 406-408.

7 a) K. J. Son, H. J. Yoon, J. H. Kim, W. D. Jang, Y. Lee and W. G. Koh, *Angew. Chem. Int. Ed.*, 2011, **50**, 11968-11971; b) H. J. Yoon, T. G. Lim, J. H. Kim, Y. M. Cho, Y. S. Kim, U. S. Chung, J. H. Kim, B. W. Choi, W. G. Koh and W. D. Jang, *Biomacromolecules*, 2014, **15**, 1382-1389; c) R. Ideta, F. Tasaka, W.-D. Jang, N. Nishiyama, G.-D. Zhang, A. Harada, Y. Yanagi, Y. Tamaki, T. Aida and K. Kataoka, *Nano Lett.*, 2005, **5**, 2426-2431; d) W.-D. Jang, K. K. Selim, C.-H. Lee and I.-K. Kang, *Prog. Polym. Sci.*, 2009, **34**, 1-23; e) W.-D. Jang, Y. Nakagishi, N. Nishiyama, S. Kawauchi, Y. Morimoto, M. Kikuchi and K. Kataoka, *J. Control. Release*, 2006, **113**, 73-79.

8 Y. Li, W.-D. Jang, N. Nishiyama, A. Kishimura, S. Kawauchi, Y. Morimoto, S. Miake, T. Yamashita, M. Kikuchi and T. Aida, *Chem. Mater.*, 2007, **19**, 5557-5562.

9 T. Pham, J. B. Jackson, N. J. Halas and T. R. Lee, *Langmuir*, 2002, **18**, 4915-4920.

10. A. Khdair, B. Gerard, H. Handa, G. Z. Mao, M. P. V. Shekhar and J. Panyam, *Mol. Pharm.*, 2008, **5**, 795-807.